P-S migration using equivalent offset method

Thais A. Guirigay and John C. Bancroft

ABSTRACT

The result of applying equivalent offset method for converted wave is presented, along with a description of the processing sequence. The quality of the method is demonstrated for the case of one real datasets. The results show superior imaging when is compared with alternative migration algorithms.

INTRODUCTION

This seismic data were acquired by CREWES in collaboration with Husky Energy, GeoKinetics, and Inova in September 2011. In addition to the seismic data, well log information with compressional and shear logs were also used. These data are from the Hussar area, Alberta, approximately 50 miles east of Calgary. The line is 4.5 kilometers and runs to NE-SW.

Acquisition

These seismic data were acquired by CREWES in collaboration with Husky Energy, GeoKinetics and Inova in September 2011. The experiment was conducted near Hussar, Alberta. Figure 1 shows the location of the study area, and the direction of the 2D line with the well locations nearby. The survey was designed to test the use of different sources and receivers, and to investigate the extension of the seismic broadband as far into the low frequency range as possible without sacrificing the higher frequencies (Isaac et al., 2011; Margrave et al., 2011). Both dynamite and Vibroseis sources with five different types of receivers were used in this experiment.

The sources included dynamite (2 kg) and two different Vibroseis: INOVA's AHV-IV (model 364), and conventional Eagle Failing Vibroseis (Y2400) with low-dwell sweep. The INOVA 364 vibrator is specially designed to operate at low frequencies. The line was shot twice with different sweeps using this vibrator: a special low-dwell sweep and a normal linear sweep, both extending from 1 to 100 Hz.

The type of receivers used were 3C 10 Hz Sensor SM7 geophones, 1C 4.5 Hz Sunful geophones, 3C Vectorseis accelerometers, Nanometrics Trillium seismometers, and 1C 10 Hz SM24 high sensitivity geophones.

The combination of all of these sources and receivers result in a quite large dataset, consisting in a total of 12 PP section and 8 P-S sections (Margrave et al., 2011).

The data were recorded to 10 seconds at sample rate of 2 msec. The line is 4.5 km long and runs NE-SW. Figure 1 shows the location of the study area, and the Hussar seismic line with the well locations nearby

The analysis to be shown is for the datasets acquired with 3C SM7 10 Hz geophones, and an INOVA 364 Vibroseis a with a custom low-dwell sweep as a source.

The sweep length was 24 seconds with a 10 second listen time. The sources spacing was 20 m and the receivers spacing was 10 m. In addition to the seismic data, well information has been included. Compressional sonic logs and shear sonic logs from a well (from 208 m to 1569 m depth) over the 2D line are also considered in this study.
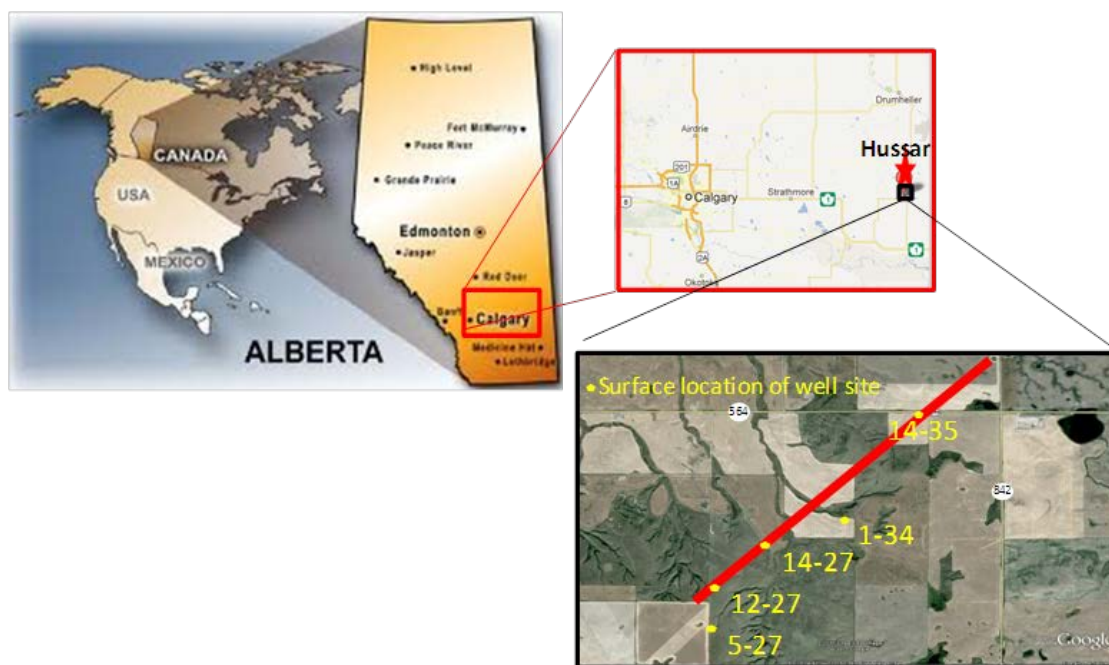

FIG 1: Area of study including the Hussar seismic line and the location of nearby wells. After Margrave et al., 2011.

Processing

The P-P and P-S radial dataset were processed at the University of Calgary by Dr. Helen Isaac at the University of Calgary through a standard processing sequence illustrated in Figure 2 and 3 respectively, using ProMAX processing software. The data was preprocessed to a horizontal datum at the mid elevation of the topography. The standard processing steps of noise removal, amplitude recovery, and deconvolution were also applied. The receiver statics of the converted wave data required special attention and were estimated by investing the lateral variability in the time events identified on the common receiver stacks (CRS) (Ion and Galbraith, 2011).

After the velocity analysis, the dataset is ported to MatLab to apply EOM code which generates CSP gathers that were then ported to Vista software for velocity analysis, NMO correction and Stack. The prestack migration is completed at this step. Figure 4 shows the flow processing for EOM data.
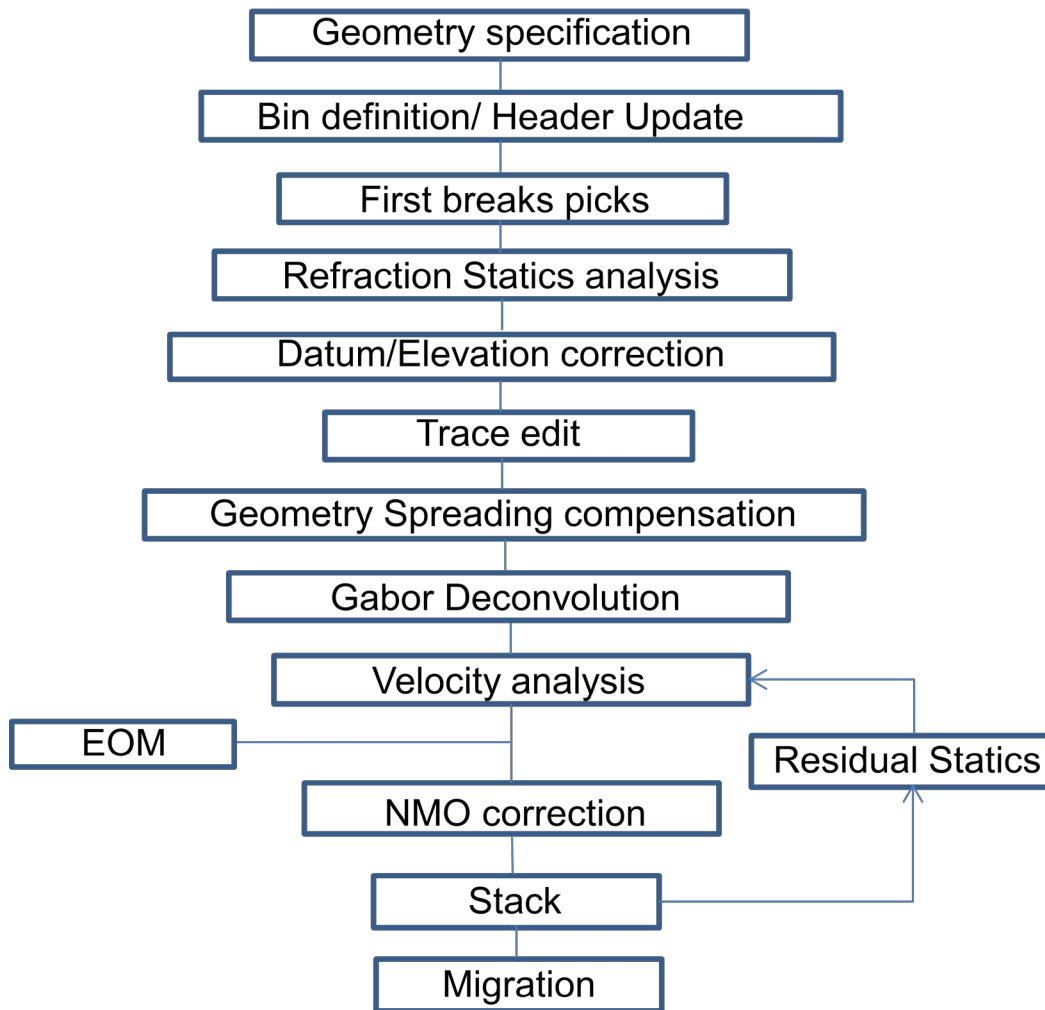
| Geometry specification |
| Bin definition/ Header Update |
| First breaks picks |
| Refraction Statics analysis |
| Datum/Elevation correction |
| Trace edit |
| Geometry Spreading compensation |
| Gabor Deconvolution |
| Velocity analysis |
| EOM | | Residual Statics |
| NMO correction |
| Stack |
| Migration |

FIG 2: Processing flow for the PP Hussar seismic dataset. (Helen Isaac, 2012 personal communication)

First estimate of V_c

There is a short range of usable data when the CMP displacement x is small, therefore a simple velocity analysis will provide a converted wave velocity V_c. (Guirigay and Bancroft, 2010)

Rotation into radial component

Asymptotic CCP binning

Geometry Spreading compensation

Import P-wave shot static and applied

Calculate and applied receiver elevation S statics

Edit bad traces

Noise attenuation: Radial filter

Gabor Deconvolution

Surface wave noise attenuation

Velocity analysis, Initial Vc

Common Receiver Brute Stack (CRS)

Estimate S-wave receiver statics from CRS

Check the CRS for additional significant receiver statics

Repeat S-wave receiver statics

EOM

PS wave Stack

Migration

FIG 3: Processing flow for the P-S Hussar seismic dataset. (Helen Isaac, 2012 personal communication)
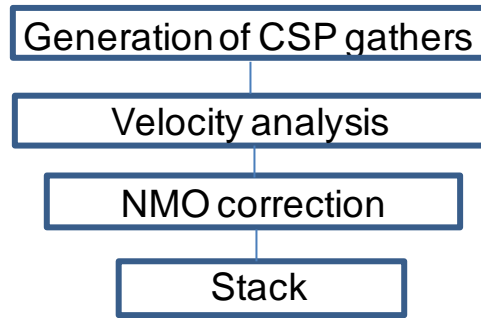
FIG 4: Processing flow for EOM.

Tests to find a best displacement *x*, a number of maximum displacements *x* were conducted using eighteen traces spaced evenly across the line. These tests were done using three methods:

1. A supergather

2. EO using a simplified equation:

$$h_e^2 = x^2 + h^2. \tag{1}$$

3. A Full EO method using the equation:

$$h_e^2 = x^2 + h^2 - \left(\frac{2xh}{tV_{mig}}\right)^2. \tag{2}$$

A derivation of these equations may be found in Bancroft et al., 1996 and 1998.

The test was repeated using values of x_{max} ranging from 25, 50, 100, 200, 400, to 800 m, and then stacked with the first estimate of $V_{c\text{-}rms}$ using the $V_{p\text{-}rms}$ velocity and $\gamma=2$. The results are shown in Figure 5 which shows the eighteen stacked traces, (micro-stack), for each x_{max}. The quality of the traces improves with increased *x* and could be used for a second estimation of V_c. However, these data are very flat and not all supergathers of this size are used, as they depend on offset.

The test was repeated using methods 2 and 3, using the same values of x_{max}, as shown in Figure 6 and Figure 7 respectively. The panel with x_{max} 100 m shows the better image of the reflectors mainly in the shallow part of the sections above 1.0 sec and tended to produce more coherent energy.
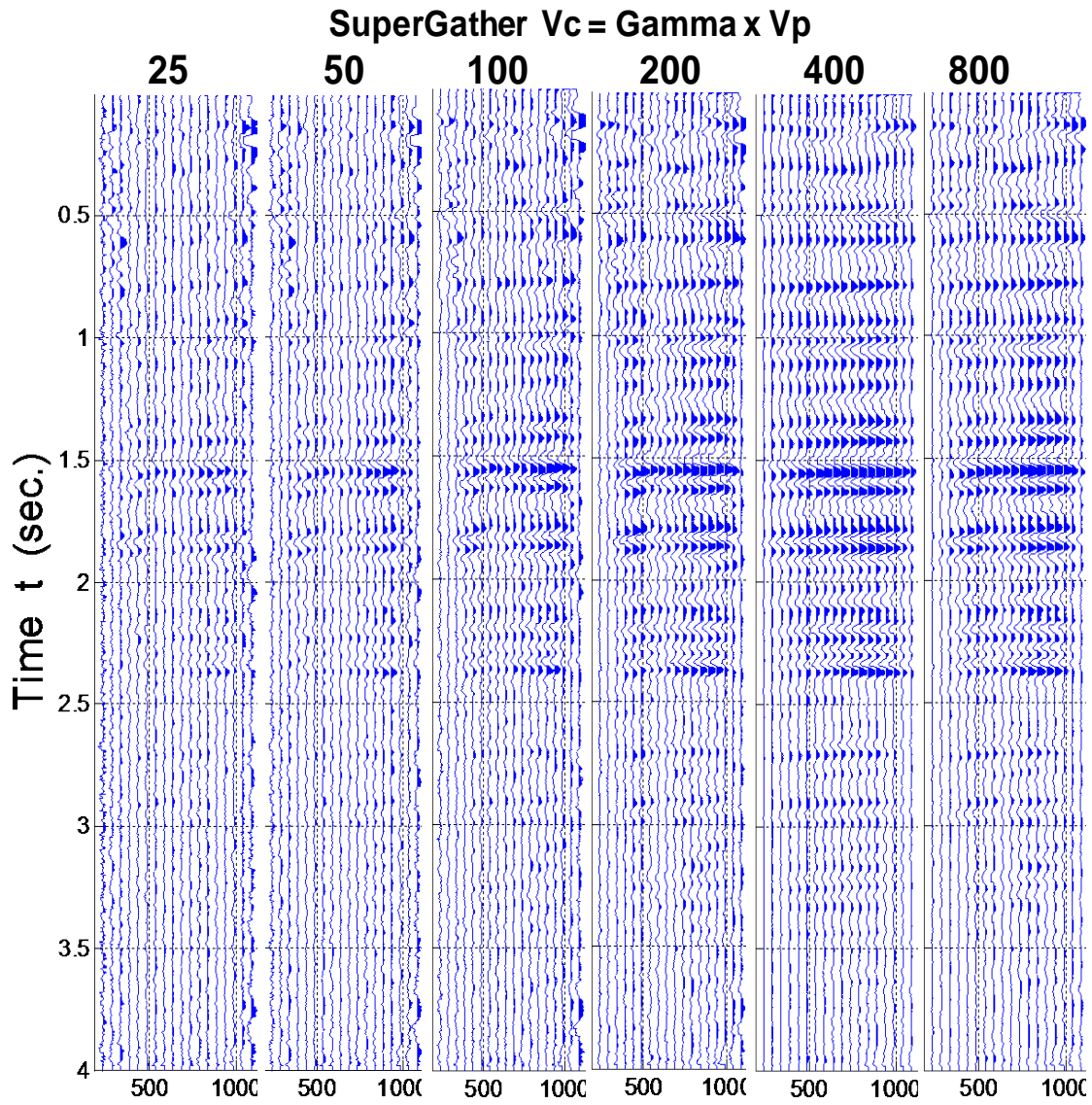
FIG 5: Six micro-stacks formed for various x_{max} as identified by the distance in meters on the top of each panel. The CSP gathers were formed using Super-Gathers. The bottom of each panel indentifies the CMP number of the stacked traces. Each panel, (micro-stack), contains eighteen traces taken at equal increments across the converted wave line.
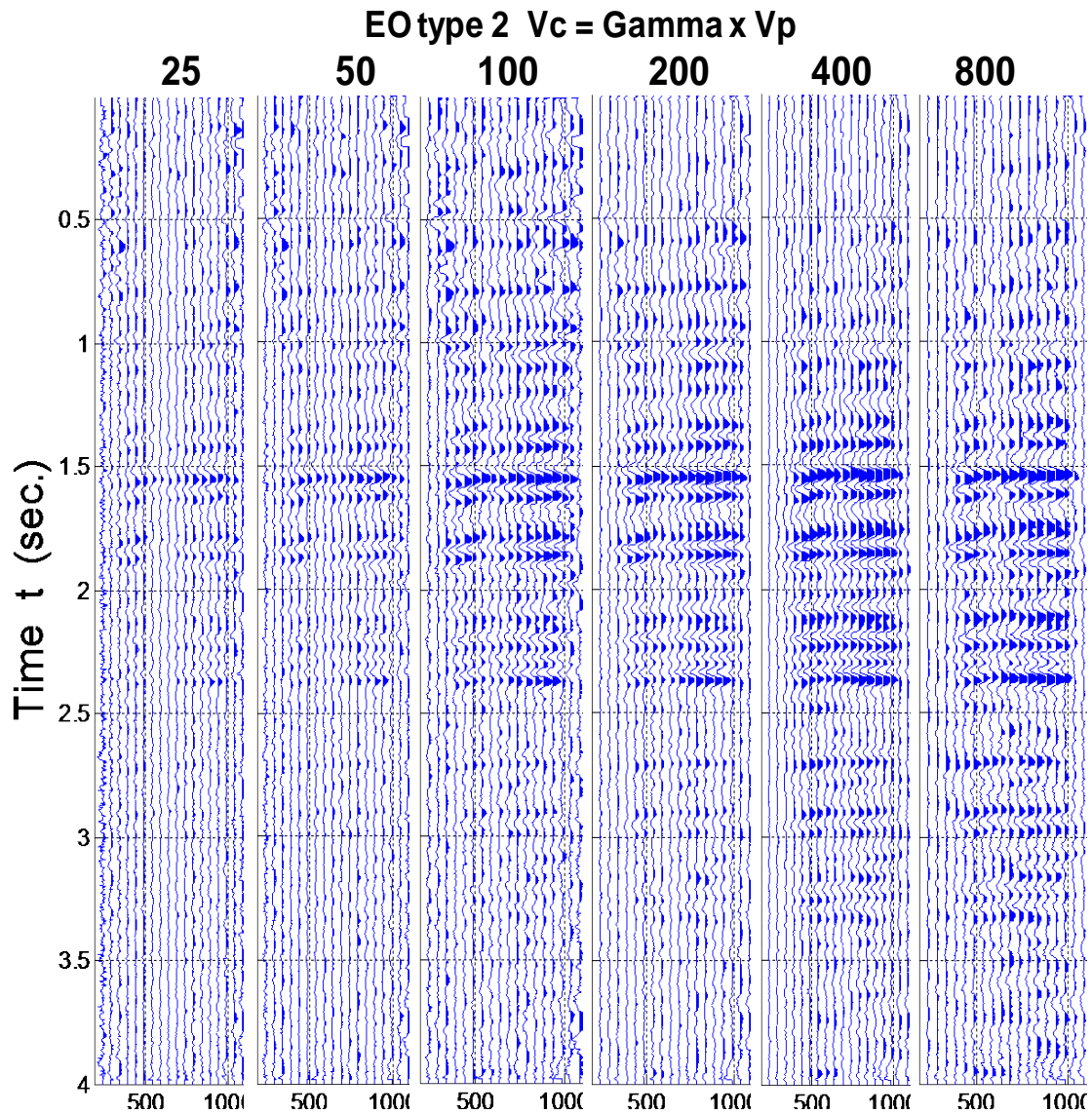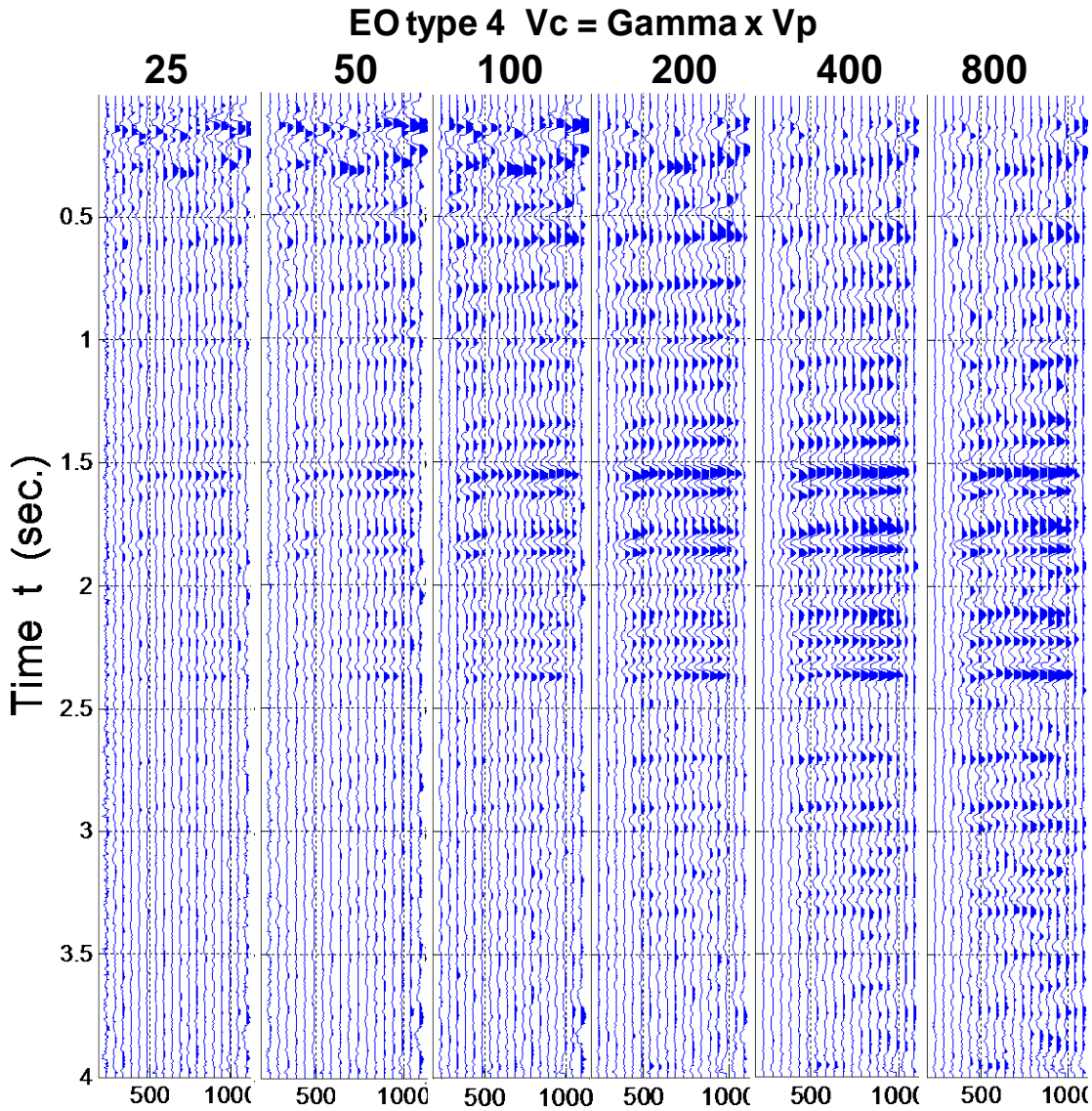
EO type 2 Vc = Gamma x Vp

FIG 6: Six micro-stacks formed for various x_{max} as identified by the distance in meters on the top of each panel. The CSP gathers were formed using simplified EOM. The bottom of each panel indentifies the CMP number of the stacked traces. Each panel, (micro-stack), contains eighteen traces taken at equal increments across the converted wave line.

EO type 4 Vc = Gamma x Vp

FIG 7: Six micro-stacks formed for various x_{max} as identified by the distance in meters on the top of each panel. The CSP gathers were formed using full EOM type 4. The bottom of each panel indentifies the CMP number of the stacked traces. Each panel, (micro-stack), contains eighteen traces taken at equal increments across the converted wave line.

An example of one limited LCCSP gather is shown in Figure 8a formed by full EO method using a maximum displacement of 100 m (x_{max} = 100 m), in the central portion of the line. The LCCSP gathers were formed and normal moveout was applied (b) using the first estimate of $V_{c\text{-}rms}$ and γ=2 using the methods described in Estimation of shear velocity from Guirigay and Bancroft, 2012 of this volume.
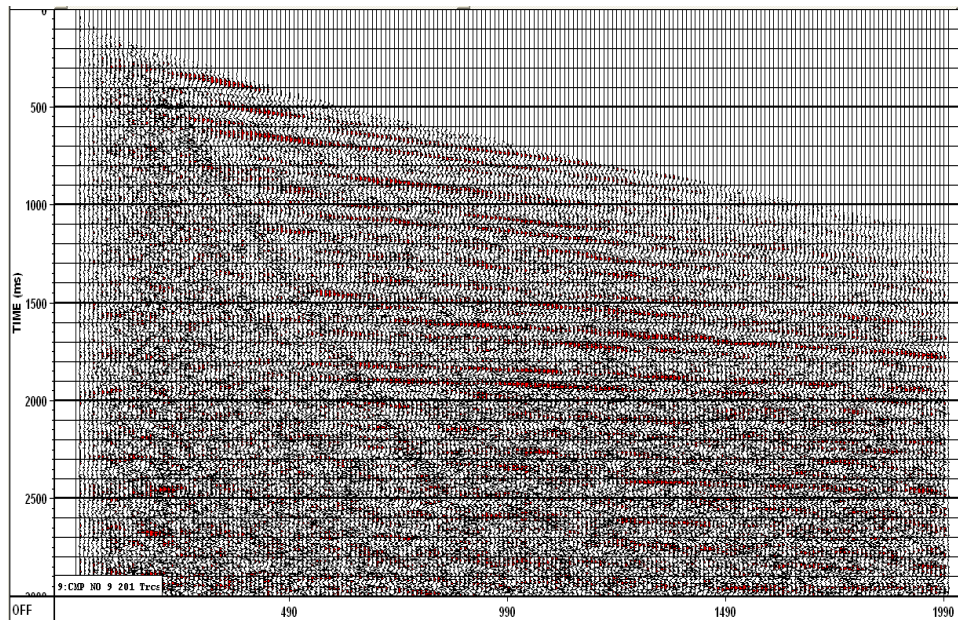
a)
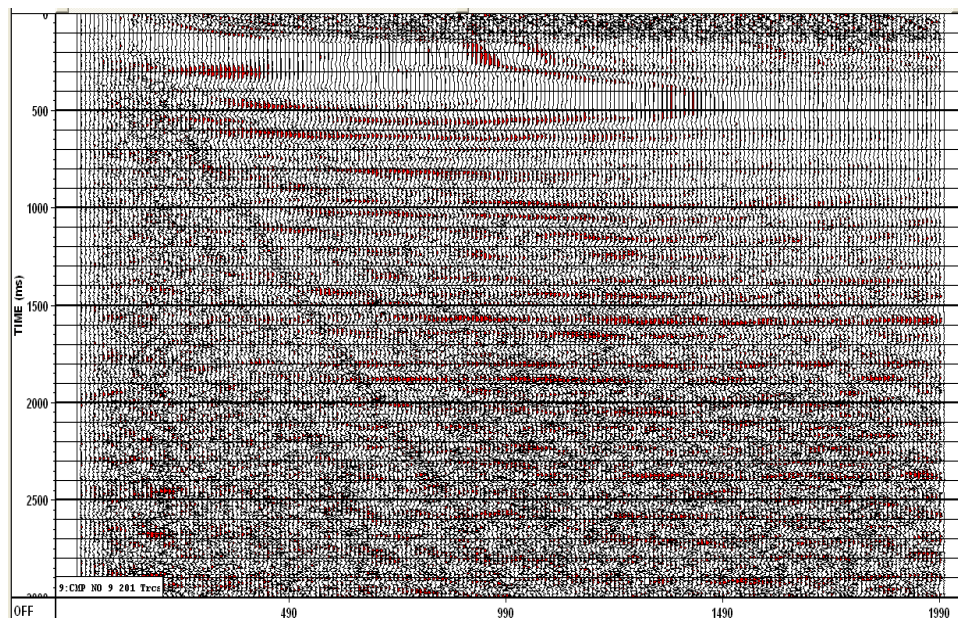
b)

FIG 8: Limited converted wave CSP gathers (LCCSP) (top) and after applied NMO
correction (bottom) formed by Full EO method

The following describes the process of forming the velocities by matching traveltimes
of the velocity procedure explained in Estimation of shear velocity from Guirigay and
Bancroft, 2012 of this volume. Figure 9a shows a comparison of P-wave velocities:
RMS, interval velocity and average velocity, $V_{p\text{-}rms}$, $V_{p\text{-}int}$ and $V_{p\text{-}ave}$. Figure 9b shows a
comparison between interval velocity for P- and C-waves, using γ=2.
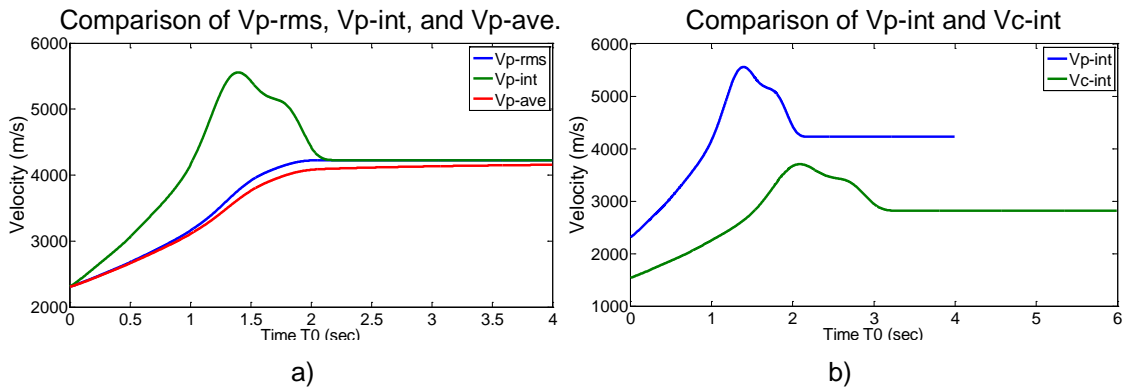
FIG 9 Sequence delineating progress from RMS P velocities to interval P and C velocities, then back to RMS C velocities. a) a comparison of P-wave velocities: RMS, interval velocity and average velocity, (b) velocity for P- and C-wave, using γ=2,

Second estimation of V_c Velocities

After an initial estimate of V_c, LCCSP gathers at a few locations allow us to get an second and improved estimate of V_c from a semblance analysis of the gathers. Figure 10 shows a semblance panel for a CSP located in the middle of the line, formed with x_{max}= 100 m and produced using (a) supergathers, (b) EO simplified, (c) full EOM methods from 0 to 4000 msec. Parts (d), (e), and (f) are the same semblance plot from 0 to 600 msec. The panels formed with the full EO method show a better focus of the energy mainly in the shallow part of the section.

Figure 11a shows a comparison of interval velocities in depth for P- and C-wave data, V_{p-int} and V_{c-int} are in blue and green respectively. Figure 11b

Velocity analysis of the LCCSP gathers produced a more accurate velocity estimate of V_{c-rms} (P) than V_{c-rms} (G) computed from V_{p-rms}. These velocities are compared in Figure 11a, showing the original V_{p-rms} velocity in blue, V_{c-rms} (G) or gamma, computed from V_{p-rms} in green, and the more accurate V_{c-rms} *(P)* or picked in red. It is interesting to note that the two converted wave velocities are equally close to a time of 1 to 1.6 sec, corresponding to the best horizontal fit of the moveout data in Figure 8. Figure 11b shows a comparison between interval velocities for P-wave and converted wave data derived from P-wave data and using γ=2 and picked from the CSPs in time (b), and (c) in depth. V_{p-int} , $V_{c-int}(G)$ from gamma and $V_{c-int}(P)$ picked are in blue, in red and in green respectively.
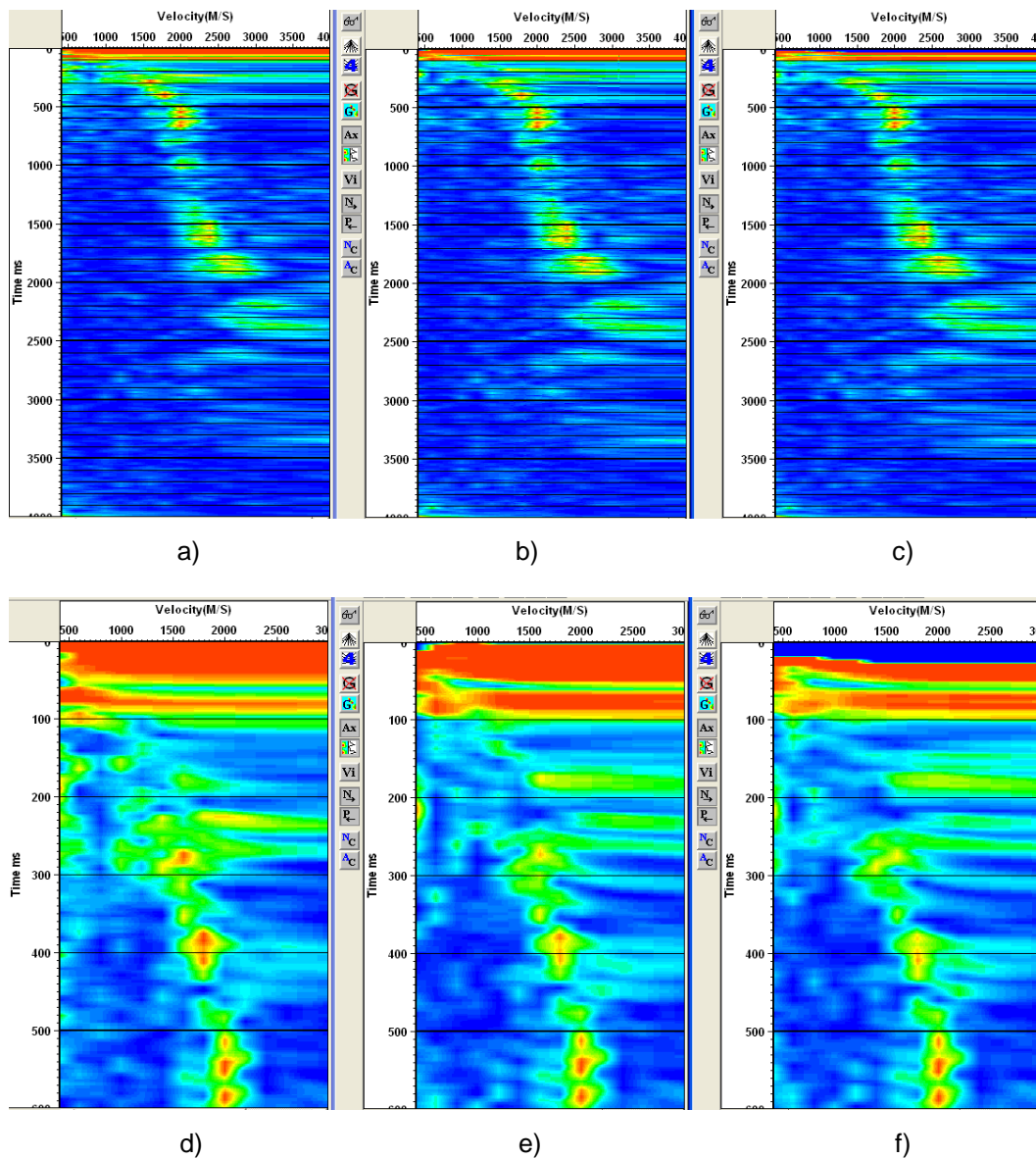
FIG 10: Three semblance panels formed with x_{max}= 100 m and from 0 to 4000 ms. The left panel a) was obtained with supergathers, b) the middle uses EO simplified, and c) the right is uses the full EO. The same semblance plots d), e), and f) are corresponding expanded views from 0 to 600 msec.
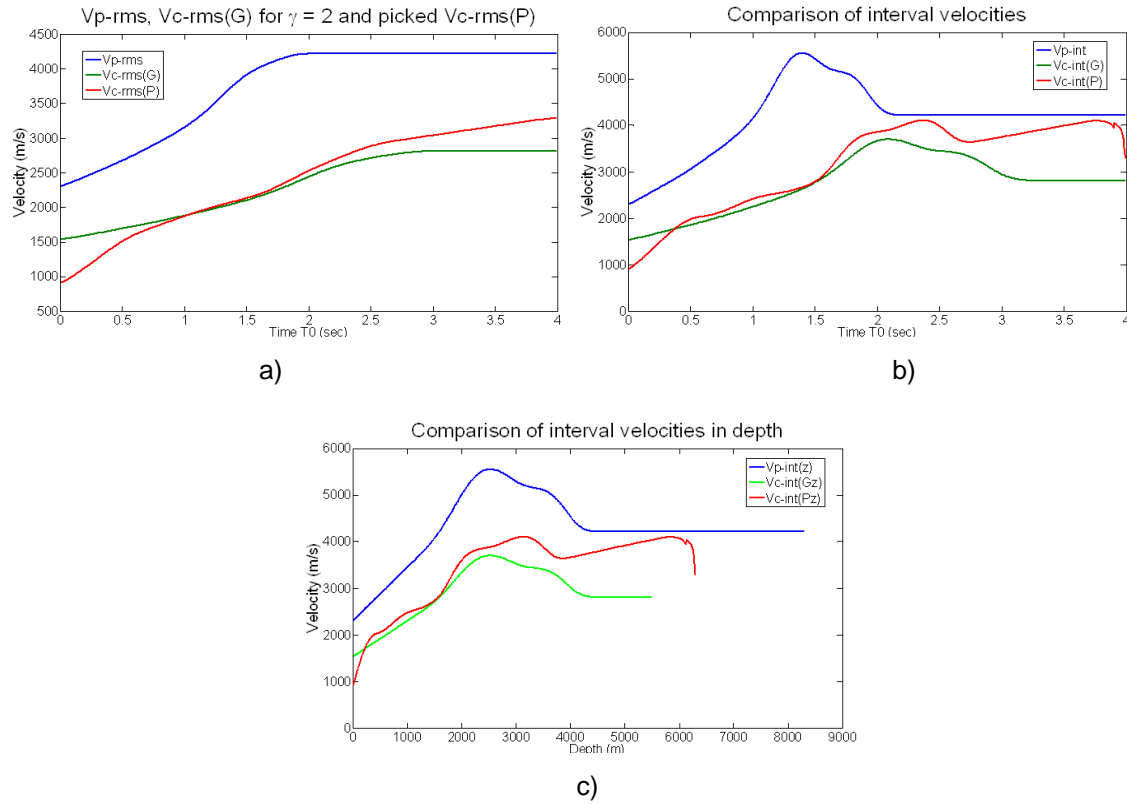
a)

b)

c)

FIG 11: a) Comparison of the velocities $V_{p\text{-}rms}$, and $V_{c\text{-}rms}$ *(G)* computed from $V_{p\text{-}rms}$, and more accurate $V_{c\text{-}rms}$ *(P),* b) Comparison between P-wave interval velocities $V_{p\text{-}Int}$, and converted wave velocities derived from P-wave using γ=2 $V_{c\text{-}Int}$ (G), and accurate $V_{c\text{-}Int}$ (P), in time, c) in depth.

Estimation of V_s Velocities

Now that an improved $V_{c\text{-}rms}$ is obtained, shear velocities can be estimated. Figure 12a shows interval velocities for P, C, and S velocities in time and the same interval velocities in depth is shown in Figure 12b. Figure 12c shows the RMS velocities for P, C, and S waves. The last velocity mentioned is shown in t_p time as the cyan curve.
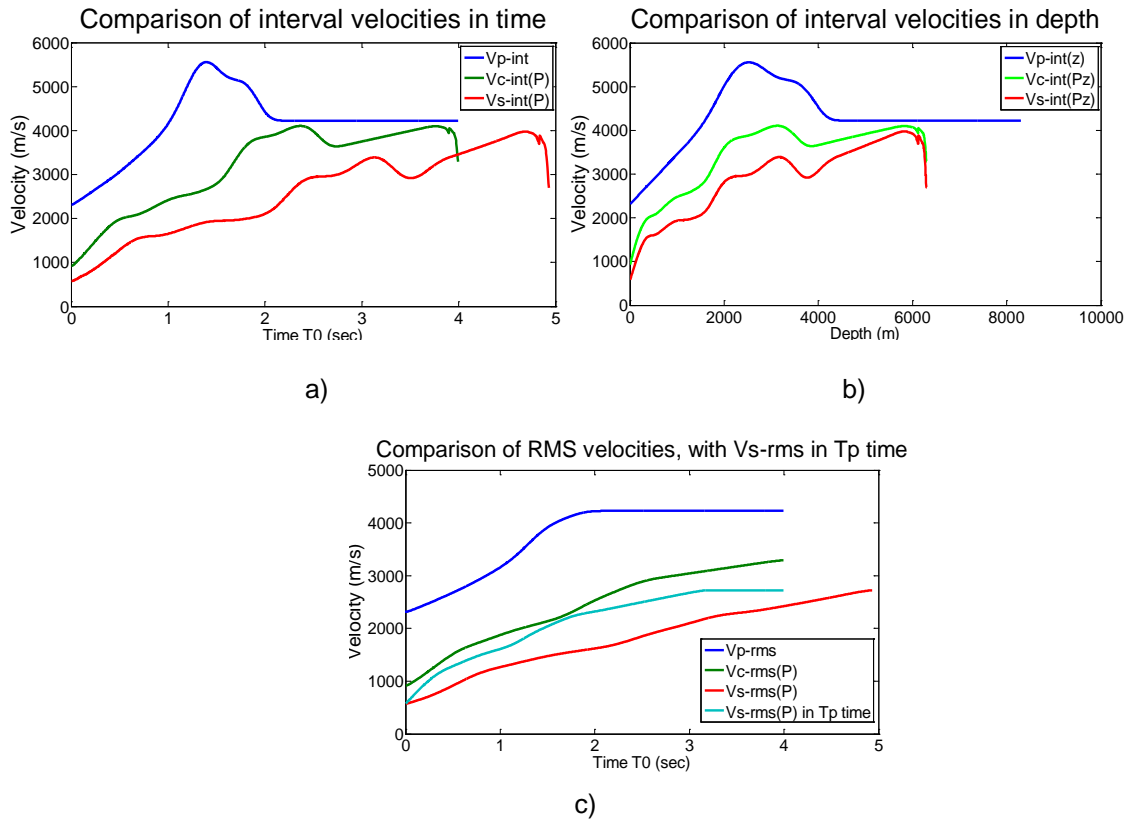
FIG 12: a) Comparison between interval velocities for P-wave V_{p-Int}, , C-wave and S-wave in time, b) the same in depth. c) Comparison of RMS velocities for P, C and S, V_{p-rms}, $V_{c-rms,}$ and V_{s-rms}.

The interval velocities derived from picked velocities are compared with velocities measurements from a well log, as illustrated in Figure 13a for P-P data, and (b) for P-S data.
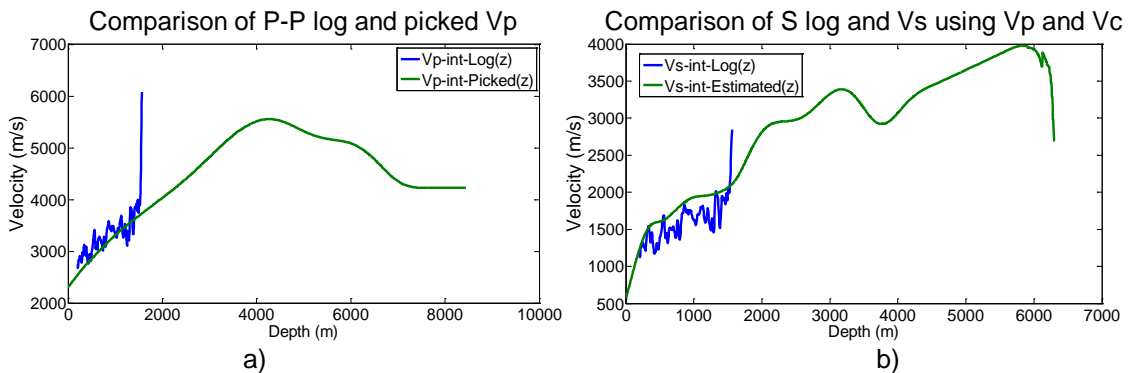

FIG 13: Comparison between interval velocities from well logs and estimated values with a) Vp and, b) Vs.

Using these interval velocities, a new estimate of γ can be obtained. The new gamma function derived from $V_{c\text{-}rms}$ from $V_{p\text{-}rms}$ using γ = 2, and from $V_{c\text{-}rms}$ picked is now ready to be compared with the logs of Well 12-27, which contains information from 208 to 1585 meters. Figure 14 shows the new estimated γ in depth and the initial γ used. The new estimate of γ tends to be higher than 2.0 near the surface, and lower than 2.0 deeper in the section as anticipated, though these are only initial estimates.
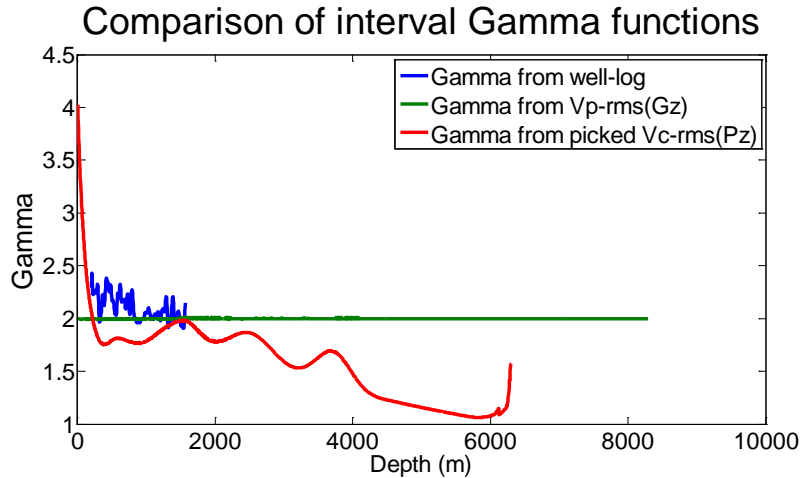
FIG 14: Comparison of estimated γ functions derived from the well logs, the assumed initial value of γ=2, and γ derived from picked P and C velocities.

Third estimation of V_c Velocities

The full EO method was applied to form all CCSP gathers using the P- and S-velocities, V_p and V_s. After the gathers were formed, new velocities $V_{c\text{-}rms}$ were picked, and NMO with a stretch mute of 60 % for P-P data and 100 % for P-S data was applied. The gathers were then stack. Figure 15a shows a CSP gather (P-P data) around in the middle of the line, with NMO applied in (b) and after applying stretch mute of 60 % in (c).

Figure 16a shows a CCSP gather (P-S data) around in the middle of the line, with NMO applied in (b) and after NMO correction and applying stretch mute of 100 % in (c).
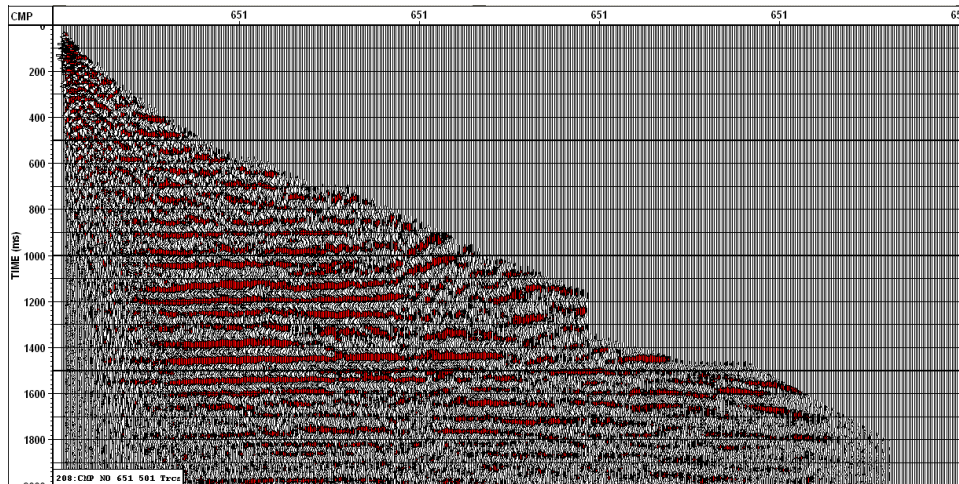
Figure 17a shows the final images of (a) the P-P and (b) the P-S sections after EOM. Figure 18a shows the P-P poststack migrated section (b) the P-S poststack migrated section, processed by Dr. Helen Isaac using a Finite Difference algorithm. The final stacked of Figure 17 and 18 have the same band pass Ormsby filter of 5-10-60-80 Hz, and the AGC gain scaling for purpose display.
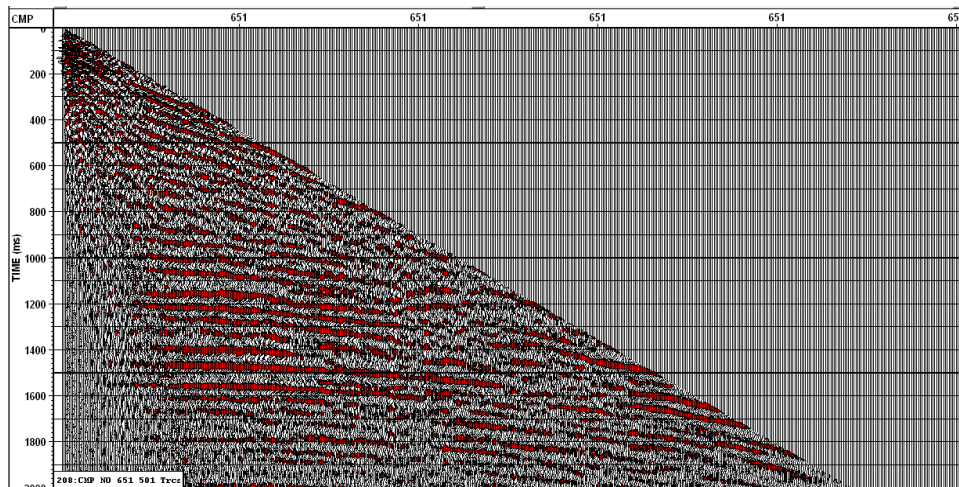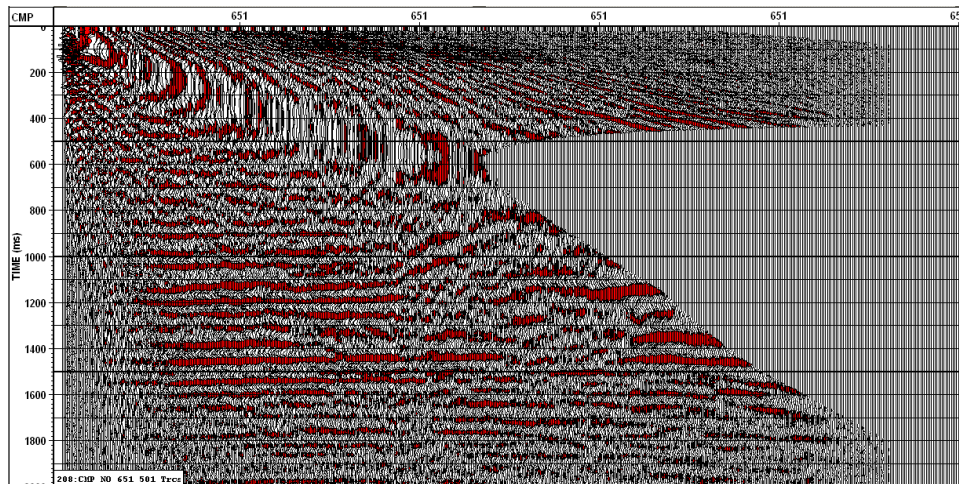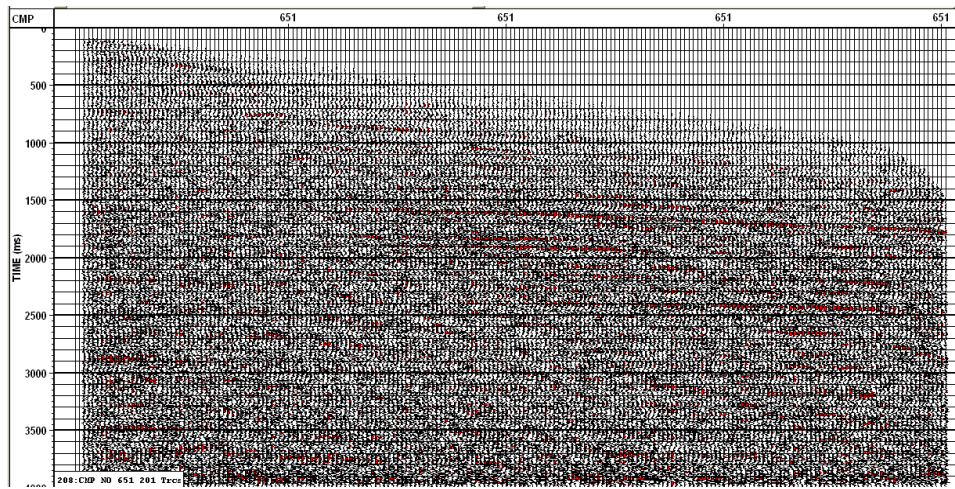
FIG 15: CSP gather in the middle of the line (a), (b) with NMO correction and, c) with NMO applied and with 60 % stretch mute applied.

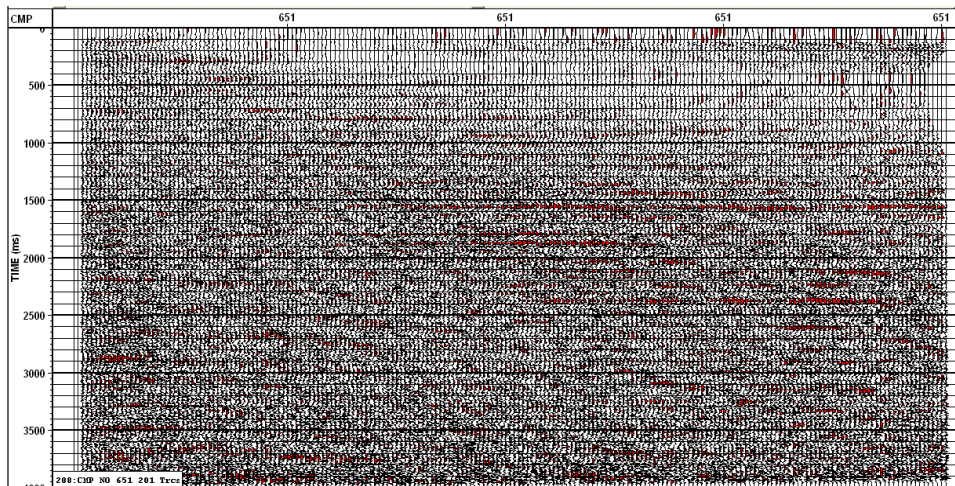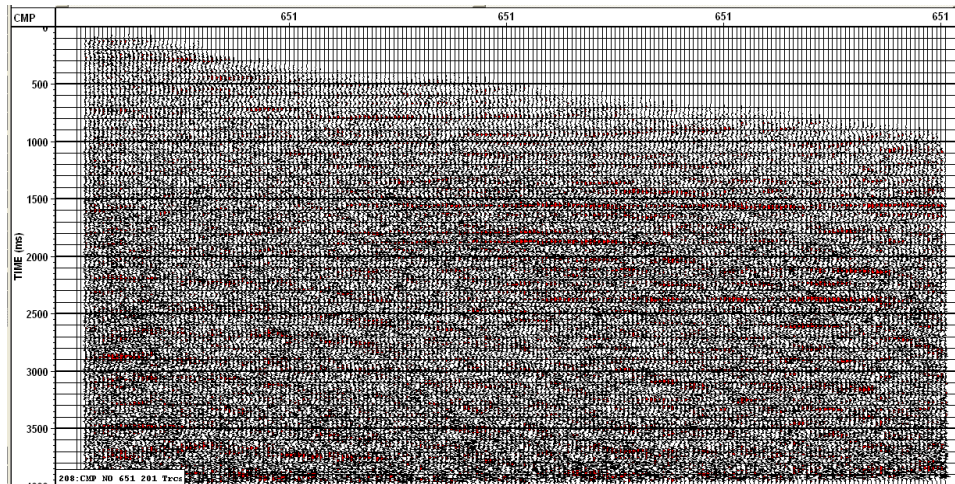FIG 16: CCSP gather in the middle of the line (a), (b) with NMO correction and, c) with NMO applied and with 100 % stretch mute applied.

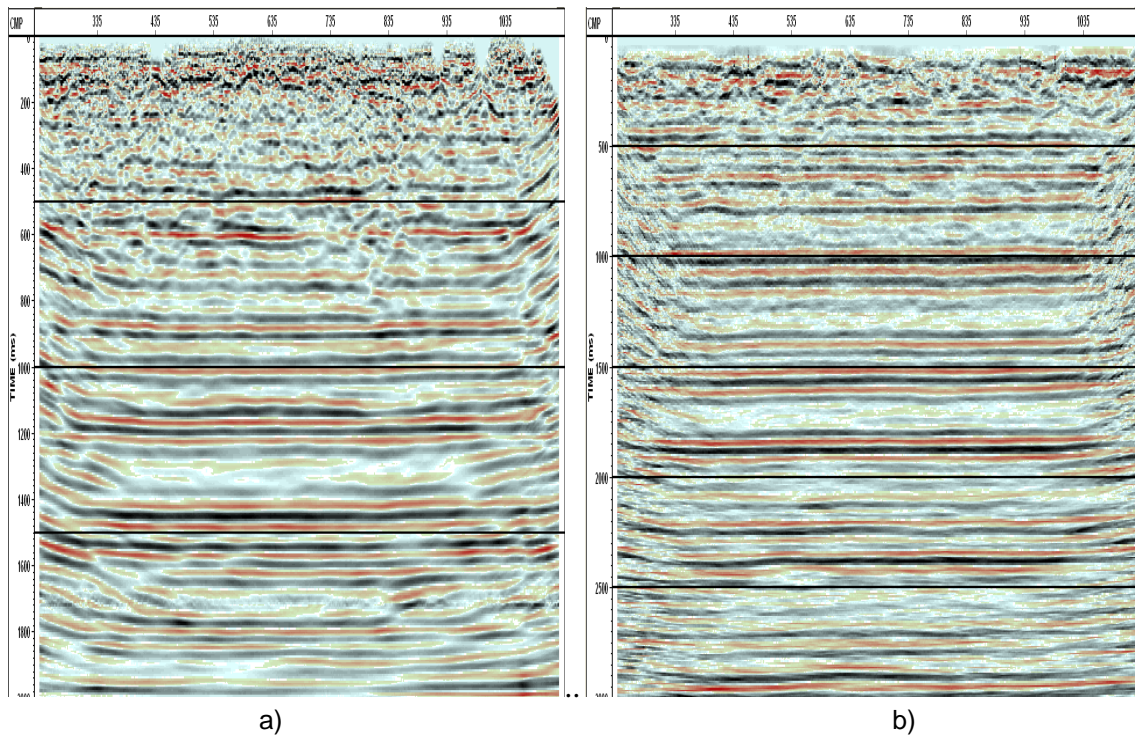a)   b)

FIG 17: a) Final stacked P-P section after EOM b) and final stacked P-S section after EOM.

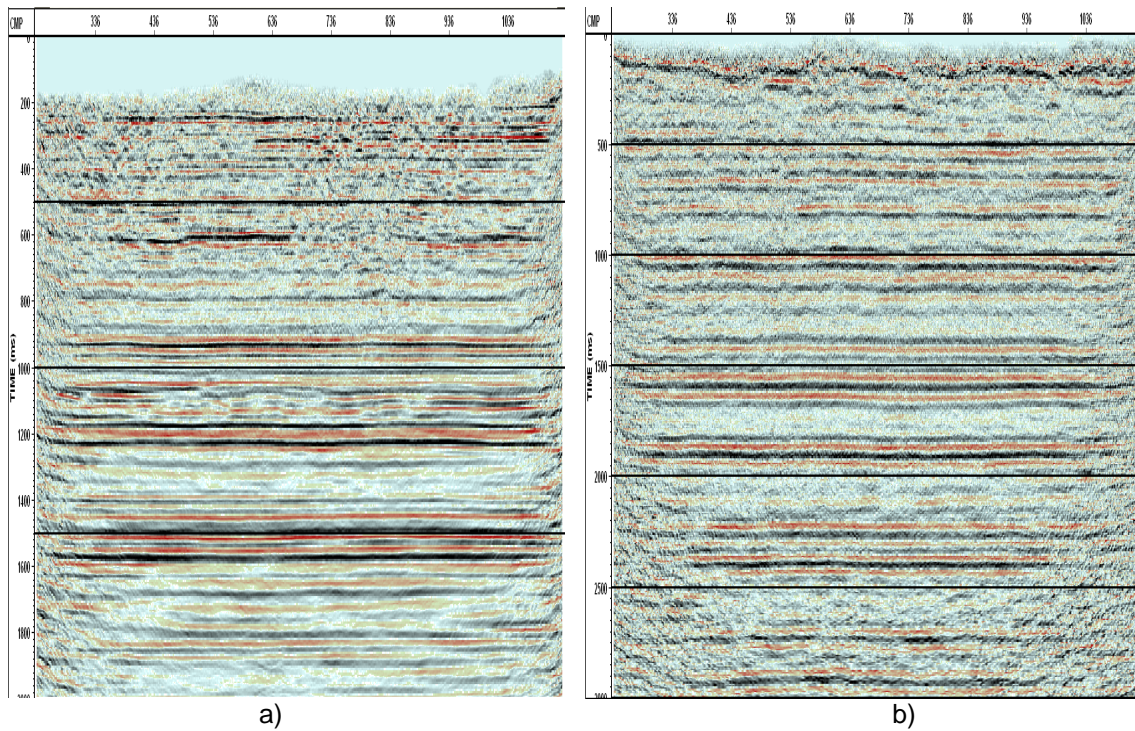a)   b)

FIG 18: Conventional processing, a) P-P poststack time migration, b) P-S poststack time migration section for comparison.

Figure 19 shows the amplitude spectrum for unfiltered final stack after EOM for (a) P-P data, and (b) P-S data.

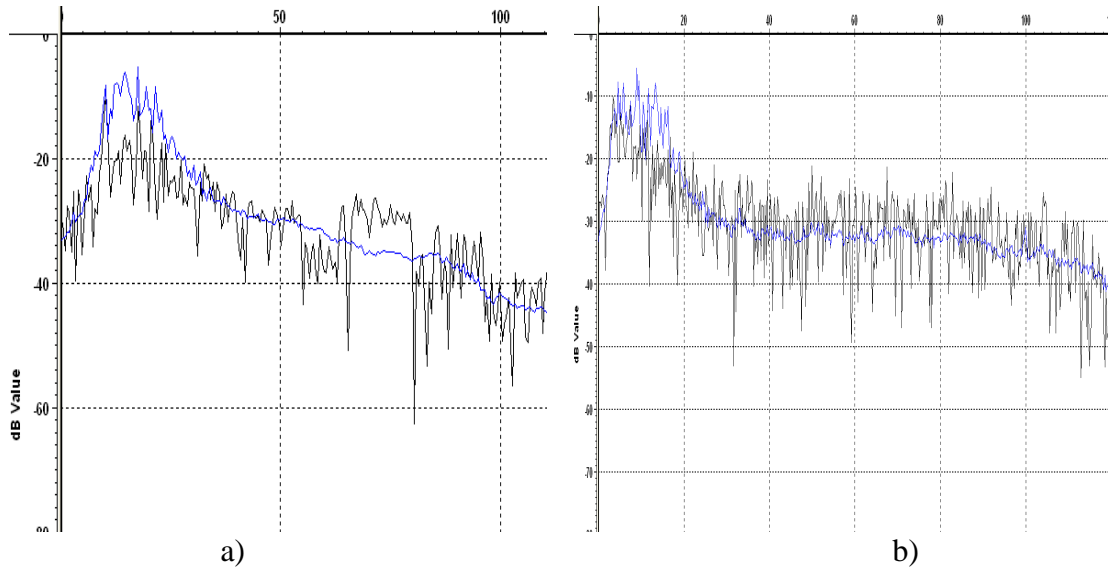a)   b)

Figure 19: Amplitude spectrum a) for final stack P-P section after EOM, and b) for final stack P-S section after EOM

Figures 20 and Figure 21 show the synthetic seismograms for compressional and shear wave respectively for the Well 12-27. The synthetic seismogram for compressional wave was generated with a wavelet 5-10-25-35 zero phase and the synthetic seismogram for shear wave was generated with a wavelet 2-4-18-22 Hz zero phase and reverse polarity for both cases.
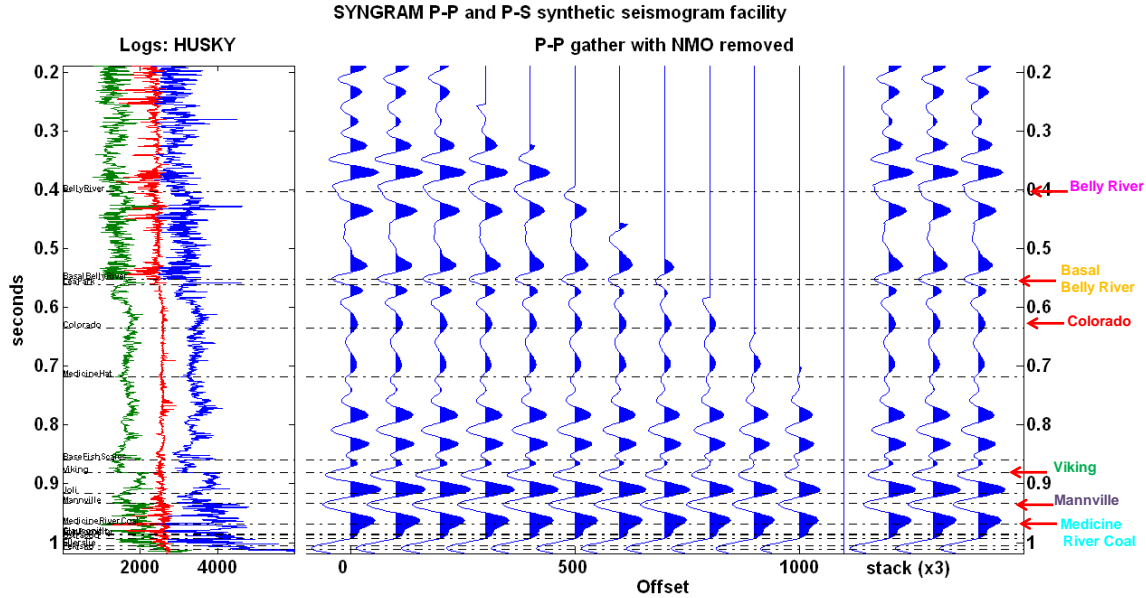

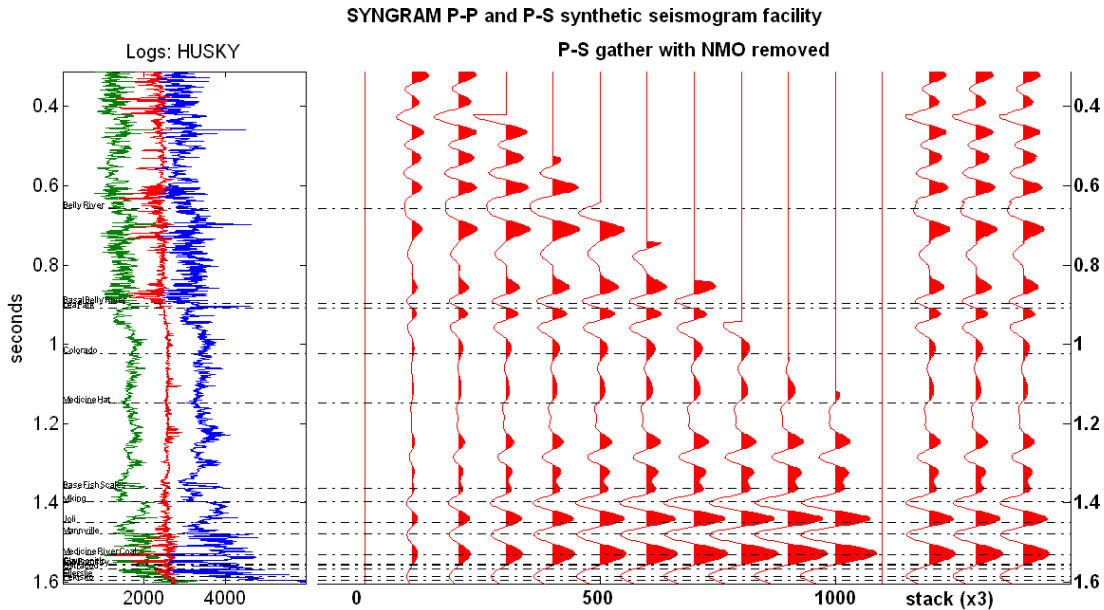FIG 20: Synthetic Seismogram from Well 12-27 for compressional wave.

FIG 21: Synthetic Seismogram from Well 12-27 for shear wave.

.

Figure 22 shows both final stack sections after EOM with P-S scaled to an approximate P-P time with synthetic seismogram and some top of geologic formations. The match between both sections is very good.
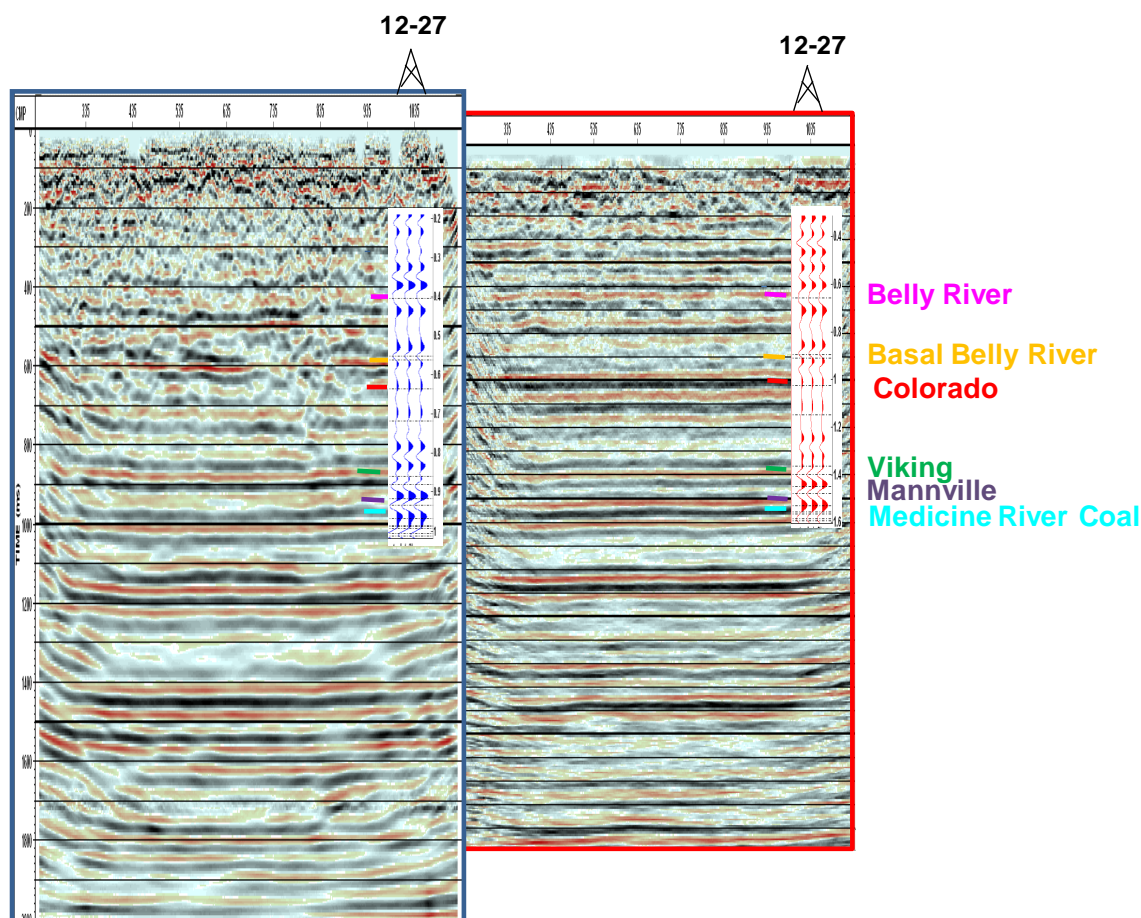
FIG 22: Final stacked P-P section after EOM (left) and Final stacked P-S section after EOM scale to P-P time with the synthetic seismograms.

CONCLUSION

Converted wave data are created using two velocities, V_p and V_s, for the incident and reflected raypaths. During different parts of the processing in this project, these two velocities were then combined into one velocity, V_c. This velocity was used first to form limited converted CSP (LCCSP) gathers that then provided an improved V_c that produces an initial estimate of V_s. Then, V_p and V_s are used to form complete equivalent offset gathers. These gathers were then analyzed to further improve V_c to provide a better moveout correction. Stacking completed the prestack migration.

Assuming a initial converted wave velocity V_c (from an initial constant value for the V_p/V_s ratio γ and RMS velocities V_p), a few LCCSP gathers were formed to provide a second estimate of the RMS velocity for converted wave V_c using the equivalent offset method.

A reasonably accurate estimate of converted wave velocities V_c is required to form CCSP gathers as part of the Equivalent Offset Migration of converted waves. These converted wave velocities (second V_c) were then used to make an initial estimate of the shear wave velocities V_s. These velocities were then used with the V_p velocities for the full prestack migration.

The common converted wave scatterpoint (CCSP) gathers were then used to create accurate estimates a third estimate V_c for moveout correction to complete the prestack migration, and to improve the estimates of V_s and γ.

The quality of the method is demonstrated for the case of Hussar dataset. The results show superior imaging when compared with alternative migration algorithms.

The estimated interval velocities of V_p and V_s are compared with velocities obtained from well-logs and compare favorably.

ACKNOWLEDGMENTS

REFERENCES

Acham, P. A., 1971, The Mannville Group (Lower Cretaceous) of the Hussar area, southern Alberta: M.S. thesis, University of Alberta, Alberta, Canada, 152 p.

Bancroft, J. C., Geiger, H. D., and Margrave, G. F., 1998, The equivalent offset method of prestack time migration: Geophysics, 63, no.6, 2042-2053.

Bancroft, J. C, Geiger, H. D., Margrave, G .F, Wang, S., and Foltinek, D. S., 1996, Prestack migration by equivalent offset and CSP gathers: CREWES Research Report, 8, 29.1-19.

ERCB, 2009, Table of formations, Alberta

Glaister, R. P., 1959. Lower Cretaceous of southern Alberta and adjoining areas. AAPG Bulletin, v. 43, No. 3, p.590-640

Guirigay, T. A., and Bancroft, J. C., 2010, Converted wave processing in the EOM domain: CREWES Research Report, 22, 23.1-24

Guirigay, T., 2012, Estimation of Shear wave velocities from P-P and P-S seismic data using Equivalent Offset Migration: M.S. thesis, University of Calgary, Alberta, Canada, 99 p

Ion, D., and Galbraith, M., 2011, A Practical Approach for Estimating Receiver Statics in 2D/3C Seismic Data Processing, Abstract for Recovery, CSEG Convention, 1-4

Isaac, J. H., and Margrave, G. F., 2011, Hurrah for Hussar! Comparison of stacked data: CREWES Research Report, 23, 55.1-23

Lynch, T. K., 2002, High resolution sequence stratigraphy and a study of Reservoir controls of the glauconitic sandstone member in the Cessford Mannville C Pool, Southeastern Alberta: M. S. thesis, University of Calgary, Alberta, Canada, 289 p.

Margrave, G. F., Mewhort, L., Phillips, T., Hall, M., Bertram, M. B., Lawton, D. C., Innanen, K., Hall, K., and Bertram, K., 2011, The Hussar low-frequency experiment: CREWES Research Report, 23, 78.1-24

Okaro, P. I., 2001, High resolution sequence stratigraphy, sedimentology, petrology, and reservoir potentials of the Glauconite Member in the Westerose and adjacent fields, Alberta, Canada: Ph. D. thesis, University of Calgary, Alberta, Canada, 352 p.

APPENDIX A: HUSSAR GEOLOGY

Hussar area is located in central Alberta Plains, approximately 50 miles east to Calgary. A generalized statigraphic column for Hussar Area, is shown is Figure A-1.

The oil sands are contained within the Lower Cretaceous Mannville Group, specifically from Glauconitic sandstone, and Upper Mannville and from Pekiski formation the Rudle Group of Mississippian age (Acham, 1971). This field is currently operated by Husky, Cenovus Energy Inc, EnCana Corporation and Oil Points Energy Ltd (2012_annual_Pool_Schedule.xls in hppt://www.ercb.ca).

The Mannville Group and stata equivalent are present over most of the Western Canada Sedimentary Basin (WCSB). This group lies unconformably above carbonates upper Paleozoic and older Mesozoic rocks and is overlain by predominantly marine shale of the Colorado Group.

Mannville Group, known as oil sands were deposited mainly fluvial environment consists of interbedded continental sand and shale in the base, followed by a calcareous sandstone member, marine shale and glauconitic sandstone. Mannville Group was divided in central Alberta into lower and upper units of implied formational status. The Upper Mannville Formation is named Glauconitic sandstone due to the presence of glauconite within marine sandstones. The Glauconite sandstone is overlying by the continental sediments of the undifferentiated Upper Mannville consisting of sandstone, siltstone, shale and coal beds and is underlying by the calcareous shale and lime beds of the marginal Ostracod member (Okaro, 2001, Lynch, 2002).
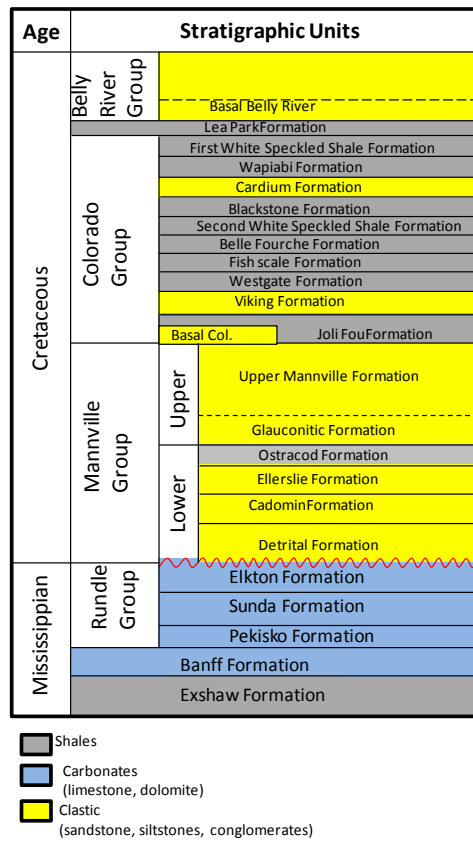
FIG A-1: Generalized bedrock stratigraphy for Hussar area. After ERCB, 2009